JGR Atmospheres

RESEARCH ARTICLE
10.1029/2020JD034082

Dynamical Differences Between Short and Long Blocks in the Northern Hemisphere

Marie Drouard[1,2], **Tim Woollings**[1], **David M. H. Sexton**[3], **and Carol F. McSweeney**[3]

[1]Atmospheric, Oceanic and Planetary Physics, University of Oxford, Oxford, UK, [2]Departamento de Física de la Tierra y Astrofísica, Universidad Complutense de Madrid, Madrid, Spain, [3]Met Office Hadley Centre, Exeter, UK

Key Points:

- Very persistent blocks are favored by cyclonic rather than anticyclonic Rossby wave breaking
- This difference in duration observed between anticyclonic and cyclonic blocks is reproduced by several coupled models
- Various transient local mechanisms, like the transient eddy feedback on the blocking high, are shown to play a role in blocking persistence

Supporting Information:

Supporting Information may be found in the online version of this article.

Correspondence to:

M. Drouard,
mdrouard@ucm.es

Citation:

Drouard, M., Woollings, T., Sexton, D. M. H., & McSweeney, C. F. (2021). Dynamical differences between short and long blocks in the northern Hemisphere. *Journal of Geophysical Research: Atmospheres*, *126*, e2020JD034082. https://doi.org/10.1029/2020JD034082

Received 12 OCT 2020
Accepted 15 APR 2021

Abstract Blocking events are persistent weather systems that strongly impact daily weather and more importantly our societies. One reason behind their strong impact is their potential long duration, as blocking events can last from 5 days up to four-five weeks. However, the mechanisms explaining this difference of duration have not been properly studied yet. Here, we investigate the differences between short blocks, which last 5 days, and long blocks, which last at least 10 days. We take a broad hemispheric and annual approach to this question, while recognizing that other specific factors may play a role in particular region and seasons. We show that long blocks often involve cyclonic Rossby wave breaking, while short blocks are equally associated with cyclonic and anticyclonic wave breaking. This main result is reproduced in a coupled climate model ensemble. The lower number of long anticyclonic blocks might be due to three main reasons: One/the anticyclone is reinforced on the downstream side during anticyclonic blocks which is less conducive to persistence; two/positive synoptic eddy feedback tends to force the mean zonal wind toward a more northward position during anticyclonic blocks, whereas it forces the mean zonal wind to the south of the block during cyclonic blocks, which has been previously shown to be associated with more persistent weather patterns; three/particularly sustained eddy feedback is needed to maintain long anticyclonic blocks.

1. Introduction

Blocks strongly impact regional weather due to their persistence (up to 4–5 weeks). They correspond to a large-scale meridional reversal of the atmospheric circulation that blocks the westerly flow (Rex, 1950). In winter, they are associated with cold spells and in summer with hot days and even heatwaves (Cattiaux et al., 2010; Röthlisberger & Martius, 2019; Schaller et al., 2018; Sousa et al., 2018).

No unique theory describing the blocking life cycle has emerged yet. This is partly due to the nature of blocking event itself, as the term "blocking" covers a wide range of weather patterns: From the clear anticyclonic or cyclonic large-scale Rossby wave breaking (Davini et al., 2012; Masato et al., 2012; Rex, 1950) to the amplified ridge showing weaker reversal (Altenhoff et al., 2008; Drouard & Woollings, 2018; Sumner, 1954). Most blocks result from a large-scale Rossby wave breaking, which corresponds to a large-scale and irreversible overturning of the geopotential contours on a pressure level. It results in the mixing of a low-latitude/high-geopotential air mass moving north and a high-latitude/low-geopotential air mass moving south. When they rotate about each other in an anticyclonic direction, we speak of an anticyclonic wave breaking and consequently of an anticyclonic block. Similarly, we speak of a cyclonic wave breaking and a cyclonic block when the two air masses rotate about each other in a cyclonic direction.

To account for these different types of blocks, different dynamical theories for block formation have emerged in the last 70 years, including large-scale and small-scale Rossby wave interaction (e.g., Austin, 1980; Charney & DeVore, 1979; Hwang et al., 2020; Legras & Ghil, 1985), rapid cyclogenesis (e.g., Colucci, 1985; Nakamura & Huang, 2018; Sanders & Gyakum, 1980), or latent-heat fluxes (e.g., Pfahl et al., 2015; Steinfeld & Pfahl, 2019). Low-frequency flow has also been shown to be more important for blocking formation over Europe, while the synoptic flow would be more important for Pacific blocks (Nakamura et al., 1997). The maintenance of blocking events has been shown to be due to positive synoptic eddy feedback (e.g., Altenhoff et al., 2008; Berckmans et al., 2013; Colucci, 1985; Mak, 1991; Shutts, 1983). Block maintenance is a key process for blocking events as it determines their duration, which has a strong impact on weather and society. Indeed, the longer a block the stronger its societal impacts. However, the reason why some blocks last

longer than others is still not well understood. It could be due to forcing by modes of variability, in particular tropical modes of variability (e.g., Cassou et al., 2005; Gollan et al., 2015; Gollan & Greatbatch, 2017; Hamill & Kiladis, 2014; Henderson et al., 2016; Henderson & Maloney, 2018; Hoskins & Sardeshmukh, 1987; Renwick & Revell, 1999; Schneidereit et al., 2012), or strong synoptic feedback. But no study has investigated specifically why some blocks last only 5 days and other 4–5 weeks.

Here, we want to better understand the reasons for such a difference in duration and the potential mechanisms involved, to be able to better characterize long blocks. Recurrent blocks (i.e., successive blocks occurring over a short period of time in the same area) will not be considered here. Our purpose is to identify common ingredients of persistent individual blocks that are independent of block location or season. To do this we will consider every block between 1957 and 2019. While there are likely regional and seasonal variations in blocking mechanisms, we prefer to start investigating this question from this broader perspective. The data and methods are introduced in Section 2. Results are presented in Sections 3–7 and discussed in Section 8.

2. Data and Methods

This work is based on the 6-h reanalysis data combining ERA-40 (Uppala et al., 2005) and ERA-Interim (Dee et al., 2011) from the European Center for Medium-Range Weather Forecasts (ECMWF) on a 0.75° × 0.75° grid. Daily averages are computed for all the data. Several fields are used: The 500-hPa geopotential (Z500), the 300-hPa zonal wind (U300), the 300-hPa meridional wind (V300), the 330K-potential vorticity (PV330K), the 330K-zonal wind and the 330K-meridional wind. Every month between September 1957 and July 2019 are used to get seasonally independent results and larger sample sizes. The fields on the 330K-theta level are used over the ERA-Interim period (January 1979–July 2019) as the PV330K is not available in ERA-40.

Daily anomalies are computed relative to the daily 1957–2019 (or 1979–2019) climatology, which is smoothed using a 5-days running mean. The high- and low-frequency components of the zonal and meridional winds are also extracted using a 2–6 days band-pass Lanczos filter, to separate the synoptic-scale and low-frequency signals (Duchon, 1979).

A brief comparison is made in Section 6 with the perturbed parameter ensemble (PPE) from the UK Climate Projections published in 2018 (UKCP18; Murphy et al., 2018). The PPE ensemble is made of 15 coupled simulations developed by the Met Office Hadley Center using the HadGEM3-GC3.0.5 model, where each member only differs in the values assigned to a set of parameters (Yamazaki et al., 2021). For the comparison, we use daily Z500 over the period January 1980 to December 1997 from the 25 members (similar to that of Yamazaki et al., 2021). The grid resolution for these data is 0.83° × 0.55°.

2.1. Detection of Blocking Events

Blocking events were detected using the two-dimensional-algorithm from Masato et al. (2013). This method looks for persistent and large-scale reversals in the Z500 meridional gradient. The daily meridional gradient at each grid point, MG_i, is:

$$\overline{Z500}_n = \frac{1}{15}\int_{\theta_0}^{\theta_0+15} Z500_i\, d\theta \tag{1}$$

$$\overline{Z500}_s = \frac{1}{15}\int_{\theta_0-15}^{\theta_0} Z500_i\, d\theta \tag{2}$$

$$MG_i = \overline{Z500}_n - \overline{Z500}_s \tag{3}$$

where θ corresponds to the latitude and θ_0 to the latitude at which the index is applied. Strictly positive values of MG_i show the presence of a large-scale reversal of the Z500 meridional gradient. A local maximum in MG_i corresponds to the block center. This block center is then tracked in the following days.

Three constraints are then applied. First, the block center must not move more than 27° in latitude and 36° in longitude between two time-steps and, second, it must lie within a 40.5° in latitude X 54° in longitude box centered on the onset block center. The tracking stops when one of these two constraints is not respected. Third, the large-scale reversal must last at least 5 days to be considered a block.

Only blocks with a block center on onset day located between 40°N and 60°N are considered, to discard typically weaker high-latitude events, like large-scale quasi-stationary lows associated with northward smaller-scale high. 3,222 blocks are detected between 1957 and 2019 and 2135 between 1979 and 2019.

Blocks are then separated into short, long and very long events. Short events last only five days, long events last 10–13 days and very long events last at least 14 days. We focus on comparing short, long and very long blocks and do not consider those of average duration (6–9 days). A duration of five days corresponds to the minimum duration of blocking events. On the contrary, blocks lasting at least 14 days are amongst the 5% longest blocks. The 10–13 days interval is used to study the long blocks that have a strong impact on temperature and precipitation, but are not extreme in terms of duration. Between 1957 and 2019, 886 short blocks, 448 long blocks and 176 very long blocks are detected. Between 1979 and 2019, there are 600 short blocks, 309 long blocks and 125 very long blocks.

2.2. Direction of Breaking Index: Separation Between Anticyclonic Block and Cyclonic Blocks

To separate anticyclonic blocks from cyclonic blocks we used the direction of breaking (DB) index developed by Masato et al. (2012). This index is computed as follows:

$$\overline{Z500_i} = (\overline{Z500_n} + \overline{Z500_s}) / 2, \tag{4}$$

$$DB = \overline{Z500_{c-1}} - \overline{Z500_{c+1}}, \tag{5}$$

with $\overline{Z500_{c-1}}$, the $\overline{Z500_i}$ value one grid point upstream of the block center and $\overline{Z500_{c+1}}$, the $\overline{Z500_i}$ one grid point downstream of the block center. A positive DB index corresponds to an anticyclonic block and a negative DB index to a cyclonic block.

Finally, we add the following condition for a block to be considered anticyclonic:

$$\overline{DB_{5days}} >= 0.5, \tag{6}$$

and cyclonic:

$$\overline{DB_{5days}} =< -0.5, \tag{7}$$

where $\overline{DB_{5days}}$ corresponds to the time-average of the DB index over the first-five days of the block. It is necessary to select only blocks with clear anticyclonic and cyclonic structures during their establishment. 690 anticyclonic blocks and 908 cyclonic blocks are detected between September 1957 and July 2019 and 463 anticyclonic blocks and 595 cyclonic blocks between January 1979 and July 2019.

2.3. E-Vectors

E-vectors point approximately in the direction of wave energy propagation (compared to the slowly varying flow), therefore they show in which direction Rossby waves propagate. They are computed as follows, using the definition from Trenberth (1986):

$$\mathbf{E} = \frac{1}{2}(V300_{HF}^2 - U300_{HF}^2)\mathbf{i}, -U300_{HF}V300_{HF}\,\mathbf{j}, \tag{8}$$

where the subscript HF represents the high-frequency flow. The divergence of **E**-vectors shows where the zonal wind is accelerated by the synoptic waves. Southward-pointing **E**-vectors are associated with synoptic

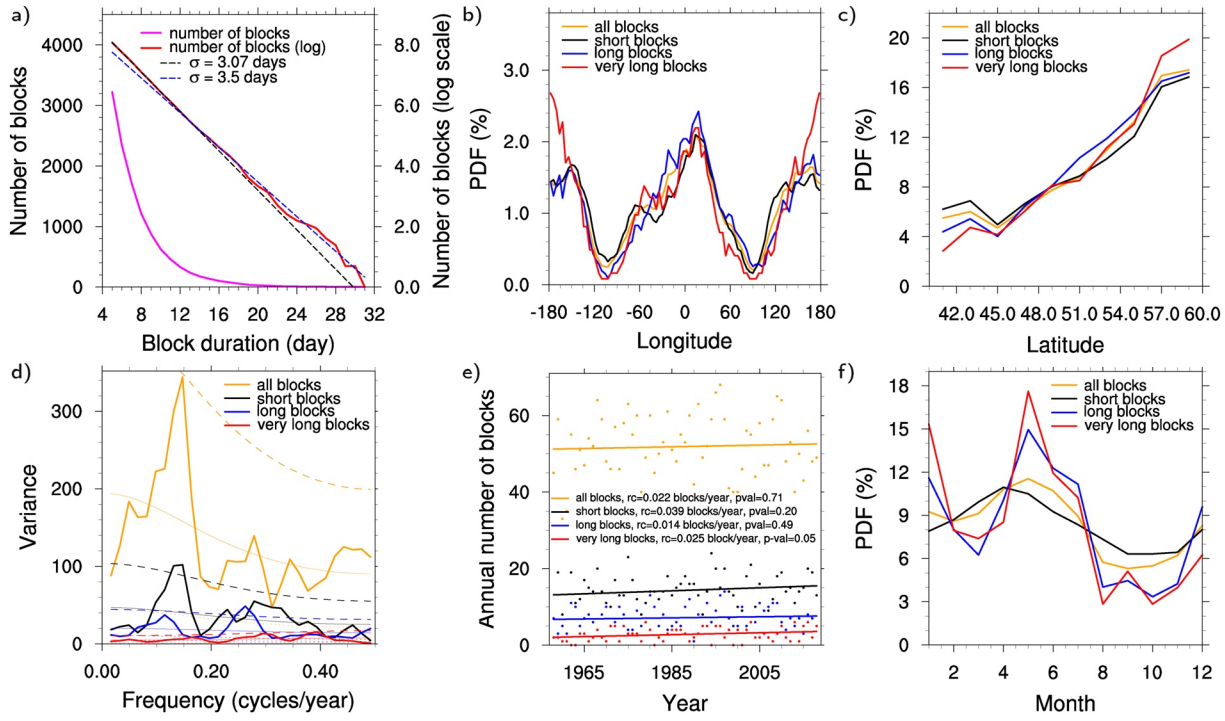

Figure 1. (a) Number of blocks lasting at least a given number of days (magenta curve). The red curve shows the same but on a log-scale. The black dash-line shows the best fit regression line for blocks lasting five to 14 days (σ = 3.07 days). The blue dash line shows the best fit regression line for blocks lasting 13–24 days (σ = 3.5 days). (b) and (c) Probability density function of blocks as a function of (b) The longitude, and (c) The latitude. (d) Power spectrum as a function of frequency (thick solid line). The power spectrum was normalized so that the area under the curve is equal to the variance of the data set after detrending. Thinner solid lines show the Markov "red noise" spectra, lines with large dashes show the 95% confidence level for the Markov spectra and lines with short dashes show the 5% confidence level. (e) Annual number of blocks (dots) and corresponding trends (solid lines). (f) Probability density function of blocks as a function of the month. For every panel, orange curves and/or dots represent the full set of detected blocks, black curves and/or dots represent the short blocks, blue curves and/or dots represent the long blocks and red curves and/or dots represent the very long blocks.

waves propagating southward and a northward transport of positive momentum that strengthens the mean flow northward where the **E**-vectors diverge. Northward pointing **E**-vectors are associated with negative momentum fluxes, which indicates a southward transport of positive momentum and so an acceleration of the jet to the south, where the **E**-vectors diverge. Here, **E**-vectors are used in association with the meridional convergence of the momentum fluxes $\left(-\frac{\partial U300_{HF}V300_{HF}}{\partial y}\right)$ to determine where the synoptic flow positively feeds back on the mean flow. A positive meridional convergence of the synoptic momentum fluxes shows where synoptic momentum is deposited and therefore where the background westerly flow is accelerated. On the contrary, the meridional divergence of the synoptic momentum fluxes shows where the synoptic eddies grow to the detriment of the background flow.

2.4. Block-Centered Composites

To create composites using every block, independently of their location, we selected every grid point in a box of 151° longitude x 61° latitude centered on the block center. We then deleted the longitude and latitude values and verified that all the block centers were co-located.

3. Distribution of Northern Hemisphere Blocks

3.1. Characteristic Time Scale

The detected blocks last between 5 and 31 days (Figure 1a). According to previous studies (D'Andrea et al., 1998; Davini & D'Andrea, 2016; Pelly & Hoskins, 2003; Masato et al., 2009), the exponential decrease seen on Figure 1a suggests that the duration of blocks is independent of the number of days it has already

lasted. However, any change in the rate of this exponential decay would imply that this hypothesis is not valid. Following Pelly and Hoskins (2003) and Martineau et al. (2017), we use a logarithmic scale to highlight changes in the rate of the exponential decay. Pelly and Hoskins (2003) defined the characteristic time scale, σ, of blocks as being the inverse of the slope of the number of blocks on the logarithmic scale: $\sigma = \frac{-1}{\alpha}$, with α, the slope of the number of blocks on the logarithmic scale. We obtain similar results to Pelly and Hoskins (2003), with a characteristic time scale of 3.07 days and a chance of 72% of an existing block lasting one more day (black dash-line). However, contrary to Pelly and Hoskins (2003), we observe a slight change in the slope of the logarithm-scale curve for blocks lasting more than 13–14 days and less than 20–22 days (red line in Figure 1a). This change of slope is associated with a characteristic time scale of 3.5 days (blue dash-line) and a chance of 75% of an existing block lasting one more day. These two characteristic timescales are significantly different as shown by a bootstrap method: The 10,000 random resamplings of the events (with replacement) gave an average characteristic timescale of 3.07 days with a standard deviation of 0.08 days for the shorter blocks and an average characteristic timescale of 3.51 days with a standard deviation of 0.28 days for the longer blocks. Therefore, longer blocks appear to have slightly higher chance to last one more day than shorter blocks. This change of slope occurs around the 95th percentile of block duration.

In the following we analyze the spatial and temporal distributions of blocks to determine if there is an obvious relation with their duration.

3.2. Spatial Distribution

As previously seen (e.g., Barriopedro et al., 2010; Masato et al., 2013; Schwierz et al., 2004), there are two main longitudinal bands of blocking occurrence: The North Atlantic-European area (60°W–60°E) and the East Asia-Pacific area (120°E–240°E; Figure 1b). Short, long and very long blocks show a longitude distribution very similar to that of all blocks (Figure 1b). The only difference observed is the strong peak in frequency for very long blocks over the North Pacific. This appears to be partly due to a cluster of extremely long blocks lasting more than 24 days (Figure S1a), which suggests that these extremely long blocks might be related to a teleconnection possibly originating in the tropical Pacific (see Breeden et al., 2020). However, despite the magnitude of this feature, very long blocks are seen to occur around much of the hemisphere.

Closer examination of Figures 1b and S1a reveal a link between the longitude of blocking and the relative occurrence of short and long events. In particular, longitudes with a low climatological blocking frequency exhibit very few long and very long blocking events. Hence, the statistics there are dominated by short events and so they have a shorter average blocking duration. This shows that the longitude of a block is statistically related to its persistence, though this is perhaps not surprising. It likely reflects that it is especially difficult to sustain a long block in a region which is climatologically less favorable to blocking overall.

Blocks are more frequent at higher latitudes (Figure 1c). Compared to the full set of blocks, short blocks tend to be slightly more frequent at lower latitudes (40°N–51°N) while long and very long blocks are more frequent at higher latitudes (north of 47°N). This is especially observed for extremely long blocks lasting at least 24 days (Figure S1b). Spatial maps of blocking frequency were also examined (not shown) but these did not reveal any spatial influence on the long and very long blocks beyond those shown in Figure 1.

We computed the ratio of the number of blocks at high latitudes (north of 50°N) to that at low latitudes (south of 50°N; Table 1). This is equal to 2.18 for the full set of blocks, 1.90 for the short blocks, 2.37 for the long blocks and to 2.98 for the very long blocks. Therefore, the latitude of the block at onset day might play a role in its duration with short blocks tending to occur at lower latitudes and long and very long blocks at higher latitudes. However, the latitude of the block alone does not fully explain the increased duration, as short blocks also occur at latitudes greater than 50°N and very long blocks at lower latitudes (south of 50°N).

3.3. Temporal Distribution

Blocks occur every year but their annual number varies from one year to another (Figure S1c). To determine if these variations exhibit preferred periods we computed the power spectrum of the annual number of blocks for each categories (Figure 1d). Only two significant peaks are observed: One for the short blocks at

Table 1
Numerical Analysis of the Link Between Blocking Duration and Blocking Latitude and Direction of Breaking

Ratios	All blocks	Short blocks	Long blocks	Very long blocks
Latitude				
$\frac{Number\ of\ high-latitude\ blocks}{Number\ of\ low-latitude\ blocks}$	$\frac{2209}{1013}=2.18$	$\frac{581}{305}=1.90$	$\frac{315}{133}=2.37$	$\frac{131}{44}=2.98$
$\frac{Observed\ latitudinal\ ratio}{Expected\ latitudinal\ ratio}$		$\frac{1.90}{2.18}=0.87$	$\frac{2.37}{2.18}=1.09$	$\frac{2.98}{2.18}=1.37$
Direction of breaking				
$\frac{Number\ of\ cyclonic\ blocks}{Number\ of\ anticyclonic\ blocks}$	$\frac{908}{690}=1.32$	$\frac{199}{232}=0.86$	$\frac{151}{91}=1.66$	$\frac{61}{29}=2.10$
$\frac{Observed\ ratio\ for\ the\ direction\ of\ breaking}{Expected\ ratio\ for\ the\ direction\ of\ breaking}$		$\frac{0.86}{1.32}=0.65$	$\frac{1.66}{1.32}=1.26$	$\frac{2.10}{1.32}=1.59$

a frequency of about 0.15 cycle/year and one for the long blocks at a frequency 0.26 cycle/year, suggesting that some inter-annual variations in short and long block frequencies might be due to external forcings. A non-significant peak at a frequency of 0.4 cycle/year is also visible for both short and very long blocks, which could correspond to a forcing by El Niño-Southern Oscillation.

Weak positive trends in the annual number of blocks are observed for each category (Figure 1e). However, only the trend for the very long blocks is significant (p-value = 0.05). It corresponds to an increase of 1.53 blocks in 61 years (between 1958 and 2018). Overall, between 1958 and 2018, no strong and significant response to global warming emerges for the annual number of blocks or the annual-mean duration in the Northern Hemisphere.

Finally, blocks are the most frequent in late spring/early summer (in agreement with Postel & Hitchman, 1999) and peak in May (Figure 1f). Their frequency decreases in summer and increases again in November. The short-block cycle is slightly in advance compared with that of the full set of blocks, as they are the most frequent in April. Long and very long blocks show a similar monthly cycle: They both peak in May and in December and both show strong frequency changes between late spring/early summer and autumn and between winter and early spring.

To summarize, these four parameters (the longitude, latitude, and year and month of occurrence) might play a role in the block duration but do not fully explain why some blocks are longer. Therefore, we will investigate the dynamics of short, long and very long blocks to look for potential differences.

4. Dynamical Overview of Short, Long and Very Long Blocks

Figure 2 shows 5-days average composites of the Z500 (black contours), U300 (magenta contours), **E**-vectors at 300hPa (blue arrows) and synoptic (high-pass) meridional convergence of the momentum fluxes at 300hPa $\left(-\frac{\partial U300_{HF}V300_{HF}}{\partial y};\text{shading}\right)$ during short blocks (left column) and during long and very long (LVL) blocks (right column). The LVL blocks are composited together because: 1/they give similar results when composited separately (not shown); 2/it allows us to have a larger sample; 3/the two composites are now of comparable size (886 blocking events for the short-block composites and 624 blocking events for the LVL-block composites).

During the 5 days preceding the blocks, no strong features are visible in the block area in either case (Figures 2a and 2b). A weak ridge is present in both cases and a beginning of cyclonic reversal is observed for the LVL blocks (black contours between −10°–0° latitude and −15°–0° longitude in Figure 2b). As a consequence, the U300 maximum shifts to the south of the future block center (Figures 2a and 2b). This southward shift appears to be driven by synoptic eddies as shown by the meridionally convergent momentum

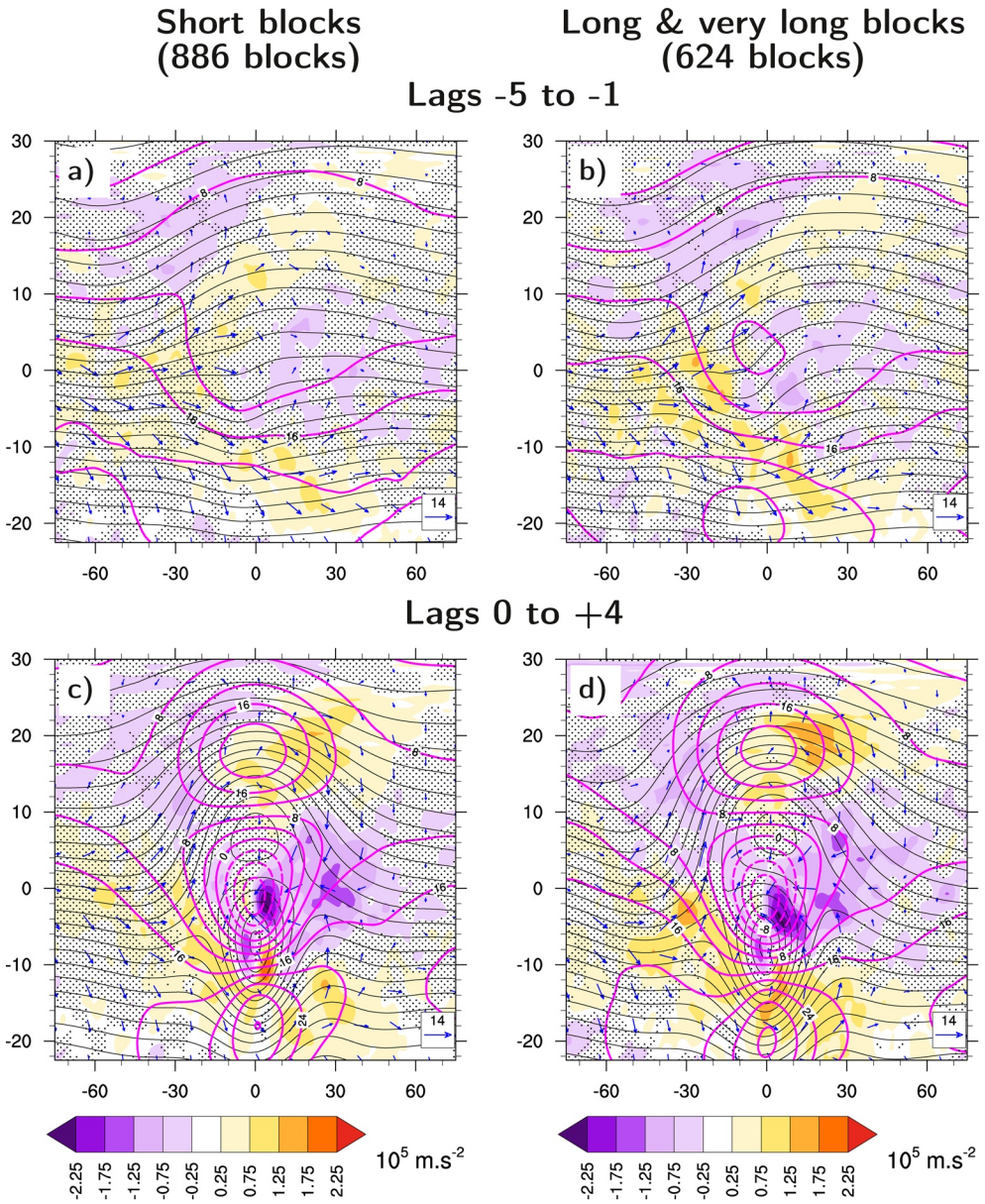

Figure 2. Five-day-average composites of Z500 (black contours, starting at 48,000 m^2/s^2 with an interval of 250 m^2/s^2), U300 (magenta contours in m/s with an interval of 4 m/s), **E**-vectors (blue arrows in m^2/s^2, scale is shown at the bottom of each panel) and synoptic momentum flux meridional convergence (shading) for the short blocks (left panels) and the LVL blocks (right panels). The composites are averaged over (a and b) the five days preceding the blocks and (c and d) the five first days of the blocks (onset day included). Non-dotted areas show where the synoptic momentum flux convergence is significant at the 95% confidence level in absolute value using a bootstrapping statistical test. LVL, long and very long.

fluxes and the strong divergent **E**-vectors around −30°–0° longitude, just upstream of the block (Figures 2a and 2b). The convergence of the momentum fluxes is slightly stronger in the case of the LVL blocks than in the case of the short blocks around −15°–0° and −30°–0° longitude (compare Figures 2a and 2b). This is associated with larger **E**-vectors. To conclude, diffluent flow, a likely precursor of the block, is observed in both cases prior to block onset and no significant differences are observed between short and LVL blocks over the five days preceding their onset.

Over the first 5 days of the blocks, a dipole structure with a high to the north of a low is observed in both cases (Figures 2c and 2d). A clear cyclonic reversal appears for the LVL blocks (black contours in Figure 2d),

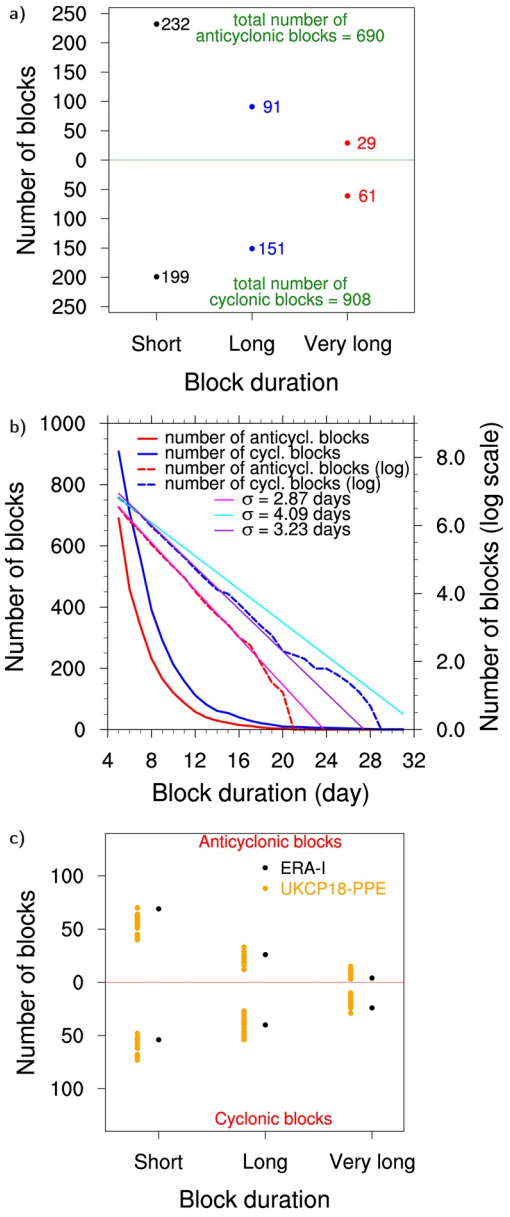

Figure 3. (a) Number of short (black dots), long (blue dots) and very long (red dots) anticyclonic (top) and cyclonic (bottom) blocks. (b) Number of anticyclonic and cyclonic blocks lasting at least a given number of days (red and blue solid curves, respectively). The thick dash red and blue curves show the same but on a log-scale. Thin lines show best fit regression for 5–16 days anticyclonic blocks (magenta), 5–8 days cyclonic blocks (cyan) and 8–21 days cyclonic blocks (purple). (c) Number of short, long and very long anticyclonic and cyclonic blocks in ERA-Interim (black dots), and in the 15-member UKCP18 ensemble (orange dots). Values above the red line shows anticyclonic blocks and values below the line cyclonic blocks. (a)–(b) The data used cover the period from September 1957 to July 2019. (c) The data used cover the period from January 1980 to December 1997.

while no particular direction of reversal or clear Ω − shape is seen for short blocks (Figure 2c). This implies that short blocks show no overall preference for anticyclonic, cyclonic and Ω − shape blocks, whereas LVL blocks seem to be dominated by cyclonic Rossby wave breaking. No strong differences are visible in the U300 field between the two composites. They both show a double-jet structure with two U300 maxima surrounding an area of negative U300 values over the block center. There are no clear differences in the strength or spatial extent of the blocks between these two composites so these factors appear to not affect the duration of blocking strongly. Similarly, no strong differences are seen in the **E**-vector orientations. However, the meridional convergence of the momentum fluxes appears slightly stronger for the LVL blocks than for the short blocks (compare Figures 2c and 2d), which could imply that the synoptic forcing is stronger for the longer blocks.

Therefore, the clearest difference observed is the preference for cyclonic Rossby wave breaking in LVL cases. To investigate this further, Figure 3a shows the number of anticyclonic and cyclonic blocks as a function of the duration. There are nearly as many anticyclonic short blocks (232) as cyclonic short blocks (199), which agrees with the absence of clear reversal direction in Figure 2c. But, there are nearly twice as many cyclonic LVL blocks (212 blocks) as anticyclonic LVL blocks (120 blocks), which explains the presence of a cyclonic reversal in the composites of the LVL blocks (Figure 2d). In addition, cyclonic blocks are equally present for the two duration categories but anticyclonic blocks are under-represented for longer durations.

This agrees with Thorncroft et al. (1993), who showed that LC1 events (i.e., anticyclonic Rossby wave breaking) were shorter than LC2 events (i.e., cyclonic Rossby wave breaking), but was not necessarily expected as Weijenborg et al. (2012) found only weak differences in terms of duration between anticyclonic and cyclonic blocks. We also observe a weak mean-duration difference between anticyclonic blocks (mean duration = 7.3 days) and cyclonic blocks (mean duration = 8.1 days). Hence, anticyclonic and cyclonic blocks have very similar mean duration, but cyclonic blocks are associated with longer extreme durations than anticyclonic blocks. We will now focus on the impact of the direction of breaking on the block duration.

5. Direction of Breaking and Block Duration

Figure 3b is the counterpart of Figure 1a but for the anticyclonic blocks and cyclonic blocks. Similarly to Figure 1a, we observe an exponential decrease of the number of anticyclonic and cyclonic blocks as a function of duration (see also Martineau et al., 2017). However, anticyclonic and cyclonic blocks show two different decay rates that also differ from the full set of detected blocks (Figure 1a). Anticyclonic blocks show a characteristic timescale of only 2.87 days, for duration of five to 16 days. This gives a chance of blocks lasting one more day of 70.5% for these durations, meaning that anticyclonic blocks are expected to be shorter on average than the full set of detected blocks.

Cyclonic blocks show longer characteristic timescales: For durations of 5–8 days, the characteristic timescale is equal to 4.09 days and for durations of 8 to 20 days, it is equal to 3.23 days (dashed blue lines and

corresponding fits). The first characteristic timescale, $\sigma = 4.09$ days, gives a chance of 78% of an existing block lasting one more day. This implies that cyclonic blocks are less prone to be short than anticyclonic blocks and then the full set of detected blocks. In addition, cyclonic short blocks represent only 22% of cyclonic blocks, while anticyclonic short blocks account for 34% of anticyclonic blocks (Figure 3a). Therefore, cyclonic short blocks tend to be under-represented compared with anticyclonic short blocks. The characteristic timescale for durations of eight to 20 days, $\sigma = 3.23$ days, corresponds to a 73% chance for an existing block to last longer, further showing that cyclonic blocks are expected to be longer than anticyclonic blocks.

Since the latitude of a block was also found to have an effect on its persistence (Figure 1c), we now examine how the latitude and direction of breaking are related. Anticyclonic blocks occur at every longitude and latitude (Figure S2). Anticyclonic short blocks seem to be particularly frequent at lower latitudes (47°N–53°N) and over Europe, as previously shown (e.g., Davini et al., 2012; Masato et al., 2012; Tyrlis & Hoskins, 2008b; Weijenborg et al., 2012). Cyclonic blocks also occur at every longitude and latitude (Figure S2). They are dominant at high latitudes (Figure S2d), from western Canada to the south of Greenland and over the North Pacific between 50°N and 60°N (e.g., Davini et al., 2012; Masato et al., 2012; Weijenborg et al., 2012). This was expected as cyclonic blocks generally occur on the poleward side of the jets, where the meridional shear is cyclonic (Peters & Waugh, 1996; Thorncroft et al., 1993; Weijenborg et al., 2012). Conversely, anticyclonic blocks occur in areas of anticyclonic meridional shear on the equatoward side of jets (Peters & Waugh, 1996).

To estimate the importance of the direction of breaking for the block duration, we computed the ratio of the number of cyclonic blocks to the number of anticyclonic (sixth row in Table 1). This is equal to 1.32 for the full set of detected blocks, 0.86 for the short blocks, 1.66 for the long blocks and 2.10 for the very long blocks. If the direction of breaking was not related to the block duration, the ratios for the three durations should be equal to 1.32. The observed ratio is 35% smaller than expected for the short blocks, 26% higher than expected for the long blocks and 59% higher than expected for the very long blocks (seventh row in Table 1). Therefore, cyclonic LVL blocks are more frequent compared with anticyclonic LVL blocks than expected and anticyclonic short blocks are more frequent compared with cyclonic short blocks than expected.

If we do the same for the observed latitudinal ratios and expected latitudinal ratios computed earlier (Section 3.2), we can see that the observed and expected ratios for the latitude are closer than for the direction of breaking (compare the fourth and seventh rows in Table 1). Hence, the direction of breaking has a stronger impact on the duration than its latitude.

6. Block Duration and Direction of Breaking in a Coupled Model Ensemble

Here, we aim at evaluating the ability of Coupled General Circulation Models (CGCMs) to capture the relation between block duration and the direction of breaking. To do this, we computed blocking event statistics for the 15 members of the UKCP18 ensemble over the period 1980–1997. Figure 3c shows the number of anticyclonic and cyclonic events for ERA-Interim and for each UKCP18 member as a function of the duration. The ensemble reproduces the results observed in the ERAI reanalysis, which further supports the above findings. It shows a strong decrease in the number of anticyclonic blocks with increasing duration and a weaker decrease in the number of cyclonic blocks with increasing duration. Consequently, anticyclonic LVL blocks are less frequent than anticyclonic short blocks and then cyclonic LVL blocks, as observed in ERA-Interim. To conclude, CGCMs are able to reproduce the relationship between block duration and the direction of breaking. This further demonstrates that, despite their known regional biases, CGCMs are able to correctly reproduce some blocking characteristics, including at least some of the dynamics which lead to extremely persistent, high-impact events.

7. Proposed Mechanisms

In this section, we investigate potential mechanisms responsible for the observed differences in block duration. To do this, we first analyze the dynamics of anticyclonic and cyclonic blocks.

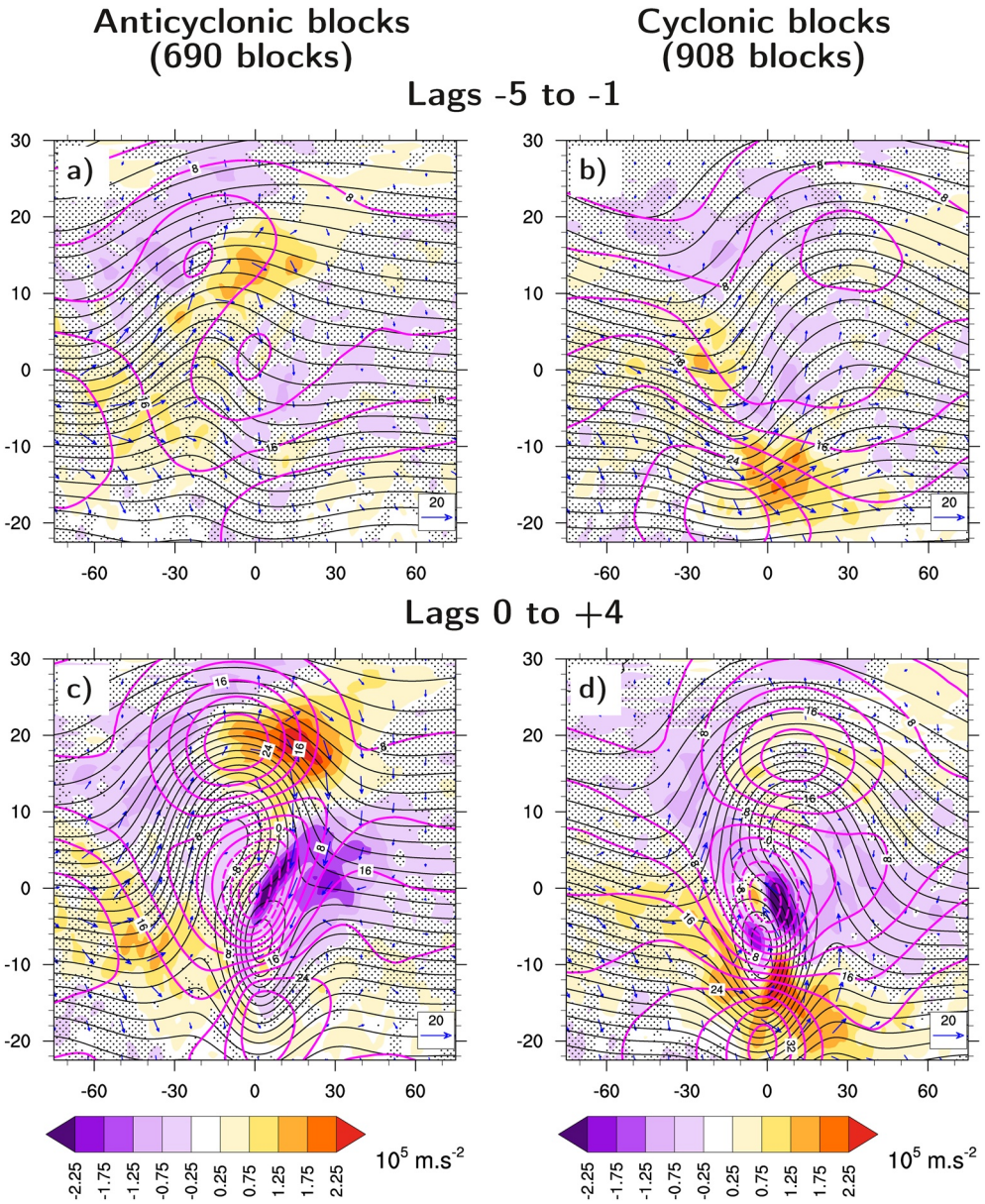

Figure 4. As in Figure 2 but for anticyclonic blocks (left column) and the cyclonic blocks (right column).

7.1. Anticyclonic and Cyclonic Blocks' Dynamics

Composites for anticyclonic and cyclonic blocks show different direction of reversal, synoptic eddy feedback and jet locations (Figures 4c and 4d). These differences are already visible prior to block onset (Figures 4a and 4b). First, a ridge is developing upstream of the future block center in the anticyclonic case, whereas, in the cyclonic case, a trough and a ridge both develop on the upstream and downstream sides of the future block center, respectively (black contours). The presence of an upstream trough and a downstream ridge in the cyclonic case prelude the future development of a cyclonic reversal. Second, the U300 (magenta contours) already splits in two in the anticyclonic case, whereas it is mostly located southward in the cyclonic case. This is associated with meridionally convergent synoptic momentum fluxes and divergent **E**-vectors upstream and to the north of the future blocks in the anticyclonic case (Figure 4a) and upstream and to the south of the future block center in the cyclonic case (Figure 4b). This shows that the synoptic eddies reinforce the U300 to the north in the anticyclonic case and to the south in the cyclonic case.

The anticyclonic and cyclonic reversals are clearly seen during the first 5 days of the blocks (black contours in Figures 4c and 4d). In both cases, a split jet appears with the characteristic northern and southern westerlies surrounding an area of easterlies (magenta contours). In the cyclonic case, the southern branch is much stronger than the northern branch (Figure 4d), whereas, in the anticyclonic case, the two branches are of nearly equal amplitude (Figure 6c). During cyclonic blocks, this is associated with strong convergent synoptic momentum fluxes and strong divergent **E**-vectors to the south of the jet. On the contrary, during anticyclonic blocks, the synoptic momentum flux convergence and **E**-vectors are weak to the south of the block and very strong to the north of blocks. Therefore, synoptic eddies strongly reinforce the U300 to the north and only weakly to the south during anticyclonic events, whereas they only reinforce the U300 to the south of the blocks during cyclonic events.

During cyclonic blocks, the strong **E**-vectors pointing northward inside the high also suggests that eddies can propagate into the ridge, which could reinforce the cyclonic block. On the contrary, during anticyclonic blocks, southward-pointing **E**-vectors are only observed on the downstream side of the high (southward pointing blue arrows between 0° and 15° longitude), which suggests that they can reinforce the block only on its downstream side. This propagation of synoptic eddies inside the block system during cyclonic events could also contribute to its larger duration. Indeed, Barnes and Hartmann (2010a) showed that the negative phase of the North Atlantic Oscillation (NAO) is more persistent partly because synoptic Rossby waves tend to break in the middle of the North Atlantic basin, where the NAO dipole is located, reinforcing both the NAO anomalies and the jet to the south. Conversely, during the positive phase of the NAO, the synoptic eddies break downstream of the NAO anomalies, which strengthens the jet northward but too far downstream to reinforce the NAO anomaly itself. Therefore, processes occurring during cyclonic blocks are very similar to those occurring during the negative NAO phase, with synoptic Rossby waves breaking to the south of the block, which reinforces the jet to the south and the blocking high to the north.

An area of strong momentum flux divergence is observed between the high and the low in both anticyclonic and cyclonic cases. In the anticyclonic case, this area is located on the downstream side of the block, whereas it is located on the upstream side of the block during cyclonic blocks. These divergent synoptic momentum fluxes on the upstream side of the block during cyclonic blocks could help maintaining the block against the westerlies, as eddies in that area extract energy from the mean flow and consequently prevent the strengthening of the mean flow to the detriment of the block. On the contrary, when synoptic momentum fluxes diverge downstream of the block, like in the anticyclonic case, it might not contribute to its maintenance.

To conclude, the spatial structure of the blocks results in different positive feedback locations. In the anticyclonic case, the high is located to the west of the low, therefore, when synoptic systems arrive in the vicinity of the blocks they are mostly diverted poleward. This is why there are strong **E**-vectors and positive momentum flux convergence to the north of the blocks. These eddies, passing north of the block, are more likely to break in a region of weak westerlies downstream and might contribute less to the maintenance of the block itself. During cyclonic blocks, the high is located on the eastern side of the block and the low on the western side. Therefore, the jet and the synoptic systems are mostly deviated southward, where they appear to reinforce both the jet and the blocking system. This explains the weaker **E**-vectors seen northward of the block in the cyclonic case.

7.2. Synoptic Eddy Feedback on the Jet Structure

As synoptic eddies have been shown to be an important parameter in block formation and maintenance (Berckmans et al., 2013; Drouard & Woollings, 2018; Green, 1977; Nakamura et al., 1997), the difference in forcing location highlighted above could explain the absence of anticyclonic blocks of extremely long duration. Therefore, maintaining the U300 to the northwest of the blocks rather than to the south of the block could be a possible reason for the shorter duration of anticyclonic blocks. According to previous studies (Barnes et al., 2010; Barnes & Hartmann, 2010a, 2010b), an equatorward located jet is more persistent than a poleward located jet, due to a weaker synoptic feedback when the jet is located at higher latitudes. Indeed, a poleward located jet is closer to the turning latitude, where the refraction index is null and, consequently, where synoptic Rossby waves are refracted southward and do not break, which inhibits the synoptic feedback (Barnes et al., 2010).

To test the role of the location of the positive synoptic feedback on the U300, we built two indices, over the period 1957–2019. They correspond to a projection of the momentum flux meridional convergence on the U300 anomaly at two locations: to the northeast of the block, where the synoptic momentum flux convergence is maximum during anticyclonic blocks (first index), and to the south of the block, where the momentum flux convergence is the strongest during cyclonic blocks (second index; see SI for more details). Contrary to what was expected, these two indices did not show any significant correlation with block duration (not shown). Strong positive synoptic feedback to the south of the block was not necessarily associated with longer blocks and strong positive synoptic feedback to the northeast of the block was not only associated with shorter blocks. However, strong positive synoptic feedback to the south of the block was mostly associated with cyclonic blocks. Therefore, while cyclonic blocks do lead to a stronger eddy maintenance of a south-shifted jet, we cannot conclude that this explains the enhanced duration of these blocks.

We also tested the hypothesis that a stronger southern jet was associated with longer events, as the southern branch appears stronger than the northern branch during cyclonic blocks. To this, we computed an index based on the difference of intensity between the southern and northern branches between 1957 and 2019 (see SI for more details). Again, the result was not conclusive and no clear difference between short and LVL blocks emerged (not shown).

The absence of conclusive results is supported by Figure 2. Indeed, Figures 2c and 2d do not show any strong difference in the momentum flux convergence and in the strength of the northern and southern branches of the U300. Therefore, taken separately, the location of the positive synoptic feedback on the U300 and the strength of the southern branch do not appear to be key parameters for block duration.

7.3. Eddy Feedback on the Blocking System

So far, we have focused on evaluating the role of synoptic eddies in maintaining the jet outside of the block region, meaning, to the south and/or to the north of the block. In this section, we investigate how the transients reinforce the blocking anomalies themselves. Following the works of Illari (1984), Mullen (1987) and Drouard and Woollings (2018), we used the convergence of the anomalous PV330K fluxes to quantify the transient eddy forcing on the high. Indeed, the convergence of the anomalous PV330K fluxes corresponds to a forcing term in the time-averaged PV equation (Illari, 1984):

$$0 = -\overline{\mathbf{v}}.\nabla\overline{q} - \overline{\mathbf{v}'.\nabla q'} \tag{9}$$

where, $\mathbf{v}$ corresponds to the wind and q to the PV330K. Overbars represent a time mean and primes a deviation from the time mean. In the areas where $\mathbf{v}$ is horizontally nondivergent, $\overline{\mathbf{v}'.\nabla q'}$ corresponds to the convergence of the anomalous PV330K fluxes.

Figures 5a and 5c show two different patterns in the convergence of the anomalous PV330K fluxes for short and LVL blocks (shading): Short blocks show an east-west dipole over the high with convergence on the upstream side of the high and divergence on its downstream side, while LVL blocks only show divergence over the whole high. Divergent anomalous PV330K fluxes induces a negative tendency in PV330K meaning a reinforcement of the ridge. Therefore, this suggests that transients, during the five first days of the block, reinforce short blocks only on their downstream side, while they reinforce LVL blocks over the whole high. This difference in the pattern of the convergence of the anomalous PV330K fluxes is even stronger between anticyclonic and cyclonic blocks (Figures 5b and 5d, respectively).

Over the low, each type of block shows a strong east-west dipole with convergence to the west and divergence to the east. The stronger signal could be due to several reasons: First, the low is located in an area of strong meridional PV330K gradient, therefore the convergence of the anomalous PV330K fluxes is stronger there and, second, the low is a more compact feature (compare Figures 5a–5d).

Figures 5e and 5f show the temporal evolution of the convergence of the anomalous PV330K fluxes, averaged in the red boxes shown in Figures 5a–5d. Short and LVL blocks both develop quickly and while short blocks weaken as quickly as they develop, LVL blocks have a much slower decay. This implies that LVL blocks are not distinct in their onset and that their longer duration is only related to their maintenance.

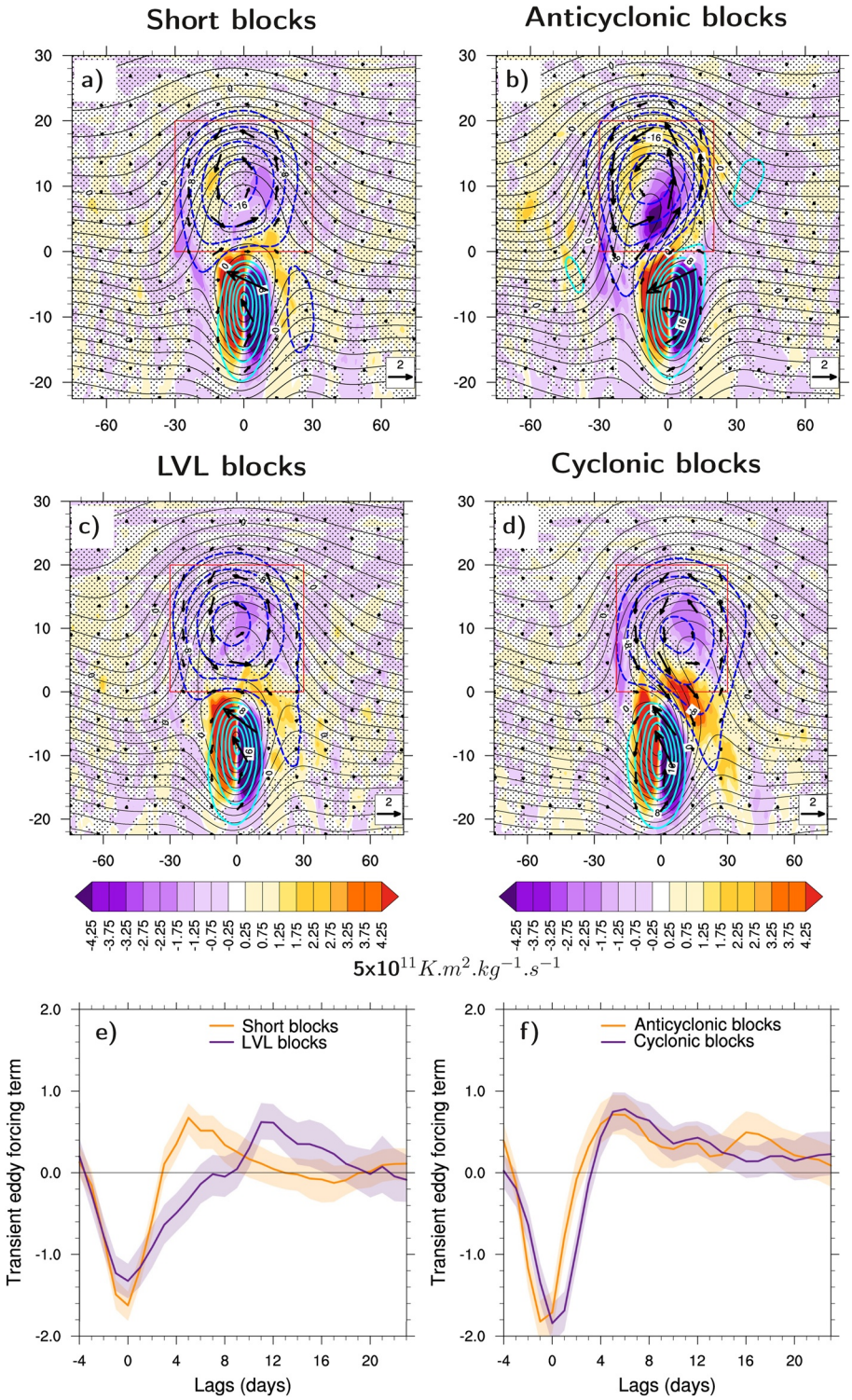
Short blocks
Anticyclonic blocks
LVL blocks
Cyclonic blocks
a)
b)
c)
d)
5x10^11 K.m^2.kg^-1.s^-1
e)
f)
Short blocks
LVL blocks
Anticyclonic blocks
Cyclonic blocks
Transient eddy forcing term
Lags (days)

The time-evolution of the transient forcing during anticyclonic and cyclonic blocks is very similar to that seen for short blocks, as shorter blocks dominate these samples (Figure 5f). However, these curves are averaged over all anticyclonic and cyclonic blocks and can't be representative of LVL anticyclonic and cyclonic blocks. Therefore, in the following, we investigate the difference between short anticyclonic and cyclonic blocks and LVL anticyclonic and cyclonic blocks.

During anticyclonic short and LVL blocks, the anomalous PV330K fluxes diverge on the downstream side and converge on the upstream side of the blocking high (Figures 6a and 6b). However, during cyclonic LVL blocks, anomalous PV330K fluxes diverge on the northern half of the high (Figure 6d), while during cyclonic short blocks, they converge on the upstream side and diverge on the downstream side of the blocking high, like anticyclonic blocks (Figure 6c).

Therefore, the placement of the anomalous PV330K divergence appears linked to the duration of the blocks. Indeed, an anomalous PV330K flux divergence over the northern half of a cyclonic block indicates that the block should develop in a LVL block. Conversely, an anomalous PV330K flux convergence/divergence dipole during a cyclonic block suggests that the block should be short.

However, two elements show that other dynamical processes play a role in blocking duration:

- First, both anticyclonic short and LVL blocks exhibit the anomalous PV330K flux convergence/divergence dipole on the high and no strong difference is observed in terms of intensity. Therefore, the difference between anticyclonic short and LVL blocks might only come from a more persistent transient forcing on the high (as shown in Figure 5e) possibly related to an external forcing.
- Second, a simple index built on the convergence of the anomalous PV330K fluxes averaged over the northern half of the blocking high did not show any correlation with block duration (see SI for more details). This was unexpected as short and LVL blocks show different patterns of anomalous PV330K flux convergence, but this could be explained by the fact that all 2135 blocks were taken into account and that the process highlighted previously might not stand for blocks of intermediate duration.

8. Summary and Discussion

Here, we investigate the differences between short and long blocks to better understand why some blocks last more than others. This question has received little attention in the literature, so we intentionally take a broad perspective, including blocks from all seasons and regions in the northern mid-latitudes. While blocking persistence is likely also shaped by regional and seasonal factors, our analysis draws out factors common to all blocks.

Our main result is that one factor does emerge as a clear influence on persistence on the hemispheric and annual scale: The direction of the Rossby wave breaking involved in the block. The latitude and longitude of the block are also seen as secondary factors (Figure 1).

Anticyclonic blocks tend to exhibit fewer extremely long durations than cyclonic blocks. However, as highlighted by Weijenborg et al. (2012), this large difference in the number of extremely long blocks is associated with small changes in the mean duration of the anticyclonic and cyclonic blocks, which are very similar.

The relation between the direction of breaking and the block duration is also observed in the coupled PPE from the MetOffice. This improves confidence in the main result saying that the direction of breaking is

Figure 5. Five-day composites of Z500 (black contours, starting at 48,000 m^2/s^2 with an interval of 250 m^2/s^2), PV330K anomaly (contours; multiplied by 10^7 $Km^2\ s^{-1}\ kg^{-1}$, navy blue dashed contours show negative values, cyan solid contours positive values and the zero contour is omitted), anomalous PV330K fluxes (black vectors multiplied by 10^5 $Km^3\ kg^{-1}\ s^{-2}$; scale is shown at the bottom of each plot) and convergence of the anomalous PV330K fluxes (shading) averaged over the first 5 days of the blocks (onset day included) for (a) Short blocks, (c) Long blocks, (b) Anticyclonic blocks and (d) Cyclonic blocks. Non-dotted areas show where the convergence of the anomalous PV330K fluxes is significant at the 95% confidence level in absolute value using a bootstrapping method. *bottom plots* Time evolution of the 3-days composites of the anomalous PV330K flux convergence (multiplied by 10^{12} $K\ m^2\ kg^{-1}\ s^{-2}$) for (e) short blocks (orange curve) and LVL blocks (purple curve) and for (f) anticyclonic blocks (orange curve) and cyclonic blocks (purple curve). The short- and LVL-block composites were averaged over the red boxes shown in panels (a) and (c) and the anticyclonic- and cyclonic-block composites were averaged over the red boxes shown in panels (b) and (d). Shaded regions in panels (e) and (f) indicate the 90% confidence interval on the mean (i.e., 5% and 95% percentiles on the mean), determined from a bootstrap. (a)–(f) The anomalous PV330K fluxes are unfiltered. The data used cover the period from January 1979 to July 2019. LVL, long and very long.

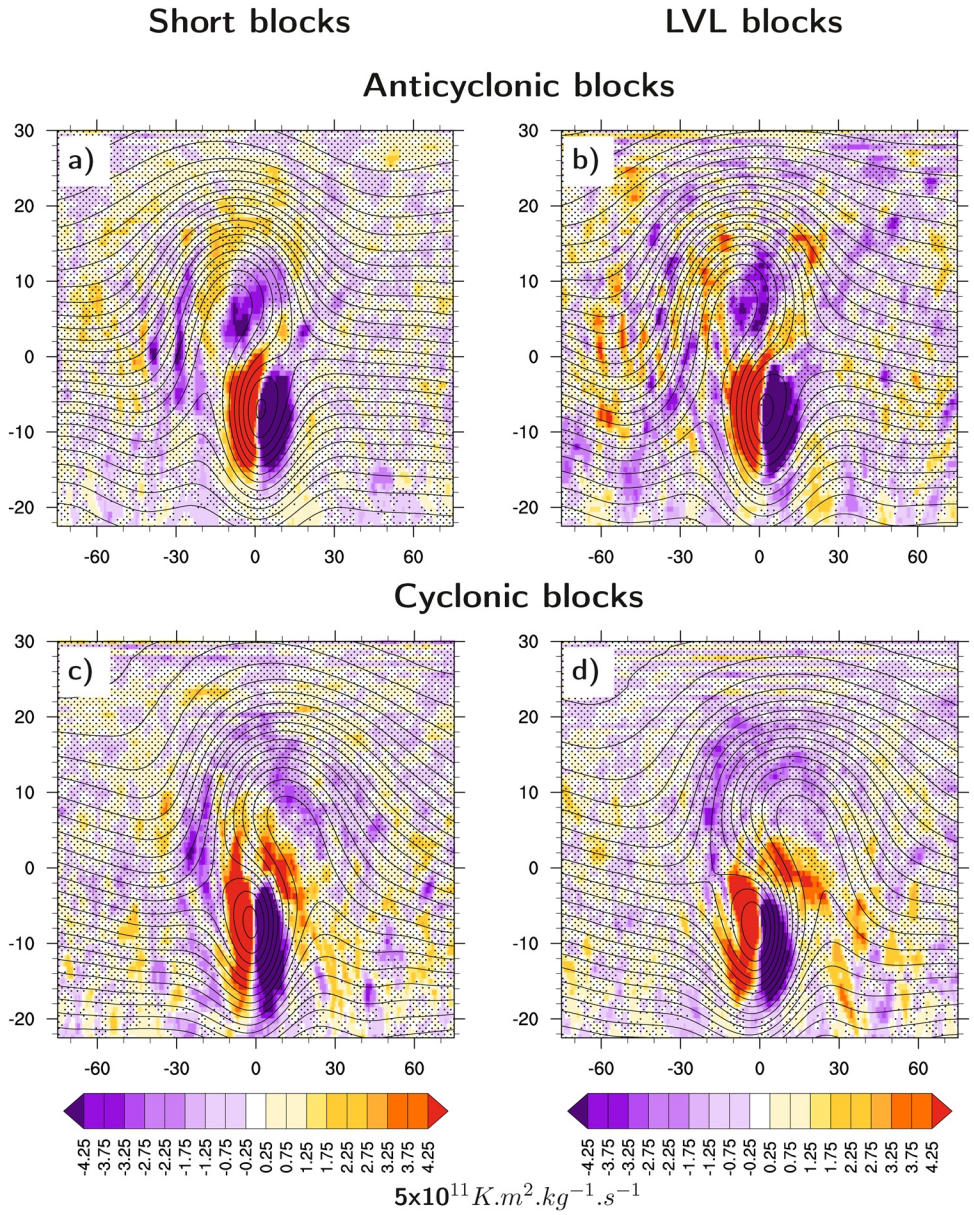

Figure 6. Five-day composites of Z500 (black contours, starting at 48,000 m^2/s^2 with an interval of 250 m^2/s^2) and convergence of the anomalous PV330K fluxes (shading) averaged over the first five days of the blocks (onset day included) for (a) the anticyclonic short blocks, (b) the anticyclonic LVL blocks, (c) the cyclonic short blocks and (d) the cyclonic LVL blocks. Non-dotted areas show where the synoptic momentum flux convergence is significant at the 95% confidence level in absolute value using a bootstrapping statistical test. The anomalous PV330K fluxes are unfiltered. The data used cover the period from January 1979 to July 2019. LVL, long and very long.

important and gives some reassurance that climate models can capture at least some of the processes involved in long blocks.

We identified three potential mechanisms that could explain the difference of duration between short and LVL and the smaller number of LVL anticyclonic blocks:

1. The location of the positive eddy feedback on the ridge. During both short and anticyclonic blocks, the ridge is reinforced by eddy PV fluxes on its downstream side. On the contrary, during cyclonic and LVL blocks, the ridge is reinforced by eddy PV fluxes on its northern half. In addition, during cyclonic short blocks the ridge is reinforced on its downstream side like during short blocks, while cyclonic LVL

blocks show the same forcing pattern as LVL blocks. This could explain why there are cyclonic short blocks. The cyclonic blocking structure has greater potential to encourage transient wave breaking in weak and/or diffluent flow upstream of the ridge. This result, based on the role of the ridge forcing is in good agreement with Illari (1984), who suggested that forcing the block on its upstream side helps to maintain it in its initial location and to avoid its advection downstream. Instead, forcing the block on its downstream side should stretch it in a south-west/north-east direction, which would weakens it, as seen for LC1 waves (Thorncroft et al., 1993). Finally, the transient forcing on the northern/upstream side of cyclonic blocks could explain the westward motion of Greenland blocks highlighted previously (Parker et al., 2019; Tyrlis & Hoskins, 2008a; Woollings et al., 2008), as Greenland blocks are mostly cyclonic.

2. The location of the positive eddy feedback on the jet. During anticyclonic blocks, synoptic eddies mostly reinforce the U300 in a northward position, which results in a strong double-jet structure. On the contrary, during cyclonic blocks, synoptic eddies reinforce the jet to the south of the block, which creates a weak double-jet structure. Following (Barnes et al., 2010; Barnes & Hartmann, 2010a, 2010b), the strong northward jet during anticyclonic blocks could explain their less extreme duration, as synoptic eddies would be less able to reinforce it, which would weaken the double-jet structure. Relatedly, Thorncroft et al. (1993) suggested that cyclonic wave breaking, occurring to the north of the jet, could last longer. Indeed, waves during LC2 progressively wrap-up cyclonically away from the jet, which inhibits decay as the wave activity has become isolated from the jet. On the contrary, waves during LC1 move progressively equatorward through the jet and progressively thin in a southwest-northeast direction to the south of the jet to become fully zonal. Despite these arguments in favor of a relation between the block and the jet location, simple indices built on the synoptic forcing location and the difference in strength of the two branches of the jet did not manage to clearly support this hypothesis. Moreover, on average, the jet structures during short and LVL blocks are very similar (compare Figures 5b and 5d). Therefore, while differences in the eddy feedbacks on the jet may play a role this does not appear to be a dominant factor.
3. The duration of the transient forcing of the high. With sustained eddy forcing some very long anticyclonic blocks can occur, despite the unfavorable structure of the block. In addition, to the blocking structure, the position of the incoming eddy activity upstream may play a role here (Drouard et al., 2013; Franzke et al., 2004).

Our results support the idea that a combination of these factors may explain the differences observed in block duration. Indeed, taken separately, because of the noise, it is difficult to show a strong correlation between any individual factor and the block duration, with the exception of the transient forcing of the high.

Another hypothesis, not tested here, involves the role of moist-diabatic processes in maintaining blocks. During cyclonic blocks, the upstream cyclone could favor the building of the ridge by enhancing the transport of lower-tropospheric PV inside the ridge via the strong release of latent heating in the warm conveyor belt (Pfahl et al., 2015). This is less likely during anticyclonic blocks, as the principal cyclone is located downstream. This is in good agreement with Steinfeld and Pfahl (2019), who showed that blocks exhibiting a strong latent heating tend to break cyclonically, while dry blocks tend to break anticyclonically. Other processes, like the forcing by tropical modes of variability (e.g., Gollan et al., 2015; Gollan & Greatbatch, 2017; Hamill & Kiladis, 2014; Henderson & Maloney, 2018; Henderson et al., 2016; Hoskins & Sardeshmukh, 1987; Schneidereit et al., 2012), or the reinforcement of the block by low-frequency eddies (e.g., Drouard & Woollings, 2018; Nakamura et al., 1997), could also contribute to the development of longer blocks. Indeed, the high number of very long block between May and July, and the case of the very long anticyclonic blocks, suggest that other dynamical processes not described here plays a role in blocking duration. Finally, other blocking indices, like those based on an anomaly method (e.g., Schwierz et al., 2004), could detect a slightly different set of events composed of more Ω-blocks, and less large-scale Rossby wave breakings, which might highlight a different balance of processes.

To conclude, this study contributes to the better understanding of blocking dynamics by identifying key ingredients for block duration. However, more work is needed to estimate the relative contribution of each ingredient mentioned above, but also to understand why cyclonic short blocks and cyclonic LVL blocks do not show the same pattern of transient forcing on the ridge.

Data Availability Statement

The ERA-40 and ERA-Interim data were downloaded on the ECMWF website: https://www.ecmwf.int/en/forecasts/datasets/archive-datasets/browse-reanalysis-datasets. Daily Z500 from the UKCP18-PPE is available by arrangement with the Met Office, please fill the enquiry form at https://www.metoffice.gov.uk/forms/contact-us-ukcp18.

Acknowledgments
The authors would like to thank three anonymous reviewers for their time and constructive comments. Marie Drouard was funded by the NERC project "Robust Spatial Projections of Real World Climate Change" (NE/N01815X/1). David Sexton and Carol McSweeney were supported by the Met Office Hadley Center Climate Program funded by BEIS and Defra.

References

Altenhoff, A. M., Martius, O., Croci-Maspoli, M., Schwierz, C., & Davies, H. C. (2008). Linkage of atmospheric blocks and synoptic-scale Rossby waves: A climatological analysis. *Tellus A: Dynamic Meteorology and Oceanography*, *60*, 1053–1063. https://doi.org/10.1111/j.1600-0870.2008.00354.x

Austin, J. F. (1980). The blocking of middle latitude westerly winds by planetary waves. *Quarterly Journal of the Royal Meteorological Society*, *106*, 327–350. https://doi.org/10.1002/qj.49710644807

Barnes, E. A., & Hartmann, D. L. (2010a). Dynamical feedbacks and the persistence of the NAO. *Journal of the Atmospheric Sciences*, *67*, 851–865. https://doi.org/10.1175/2009jas3193.1

Barnes, E. A., & Hartmann, D. L. (2010b). Testing a theory for the effect of latitude on the persistence of eddy-driven jets using CMIP3 simulations. *Geophysical Research Letters*, *37*. https://doi.org/10.1029/2010gl044144

Barnes, E. A., Hartmann, D. L., Frierson, D. M., & Kidston, J. (2010). Effect of latitude on the persistence of eddy-driven jets. *Geophysical Research Letters*, *37*. https://doi.org/10.1029/2010gl043199

Barriopedro, D., García-Herrera, R., & Trigo, R. M. (2010). Application of blocking diagnosis methods to general circulation models. Part I: A novel detection scheme. *Climate Dynamics*, *35*, 1373–1391. https://doi.org/10.1007/s00382-010-0767-5

Berckmans, J., Woollings, T., Demory, M.-E., Vidale, P.-L., & Roberts, M. (2013). Atmospheric blocking in a high resolution climate model: Influences of mean state, orography and eddy forcing. *Atmospheric Science Letters*, *14*, 34–40. https://doi.org/10.1002/asl2.412

Breeden, M. L., Hoover, B. T., Newman, M., & Vimont, D. J. (2020). Optimal north Pacific blocking precursors and their deterministic subseasonal evolution during boreal winter. *Monthly Weather Review*, *148*(2), 739–761. https://doi.org/10.1175/mwr-d-19-0273.1

Cassou, C., Terray, L., & Phillips, A. S. (2005). Tropical Atlantic influence on European heat waves. *Journal of Climate*, *18*, 2805–2811. https://doi.org/10.1175/jcli3506.1

Cattiaux, J., Vautard, R., Cassou, C., Yiou, P., Masson-Delmotte, V., & Codron, F. (2010). Winter 2010 in Europe: A cold extreme in a warming climate. *Geophysical Research Letters*, *37*. https://doi.org/10.1029/2010gl044613

Charney, J. G., & DeVore, J. G. (1979). Multiple flow equilibria in the atmosphere and blocking. *Journal of the Atmospheric Sciences*, *36*, 1205–1216. https://doi.org/10.1175/1520-0469(1979)036<1205:mfeita>2.0.co;2

Colucci, S. J. (1985). Explosive cyclogenesis and large-scale circulation changes: Implications for atmospheric blocking. *Journal of the Atmospheric Sciences*, *42*, 2701–2717. https://doi.org/10.1175/1520-0469(1985)042<2701:ecalsc>2.0.co;2

D'Andrea, F., Tibaldi, S., Blackburn, M., Boer, G., Déqué, M., Dix, M., et al. (1998). Northern Hemisphere atmospheric blocking as simulated by 15 atmospheric general circulation models in the period 1979–1988. *Climate Dynamics*, *14*(6), 385–407.

Davini, P., Cagnazzo, C., Gualdi, S., & Navarra, A. (2012). Bidimensional diagnostics, variability, and trends of Northern Hemisphere blocking. *Journal of Climate*, *25*, 6496–6509. https://doi.org/10.1175/jcli-d-12-00032.1

Davini, P., & D'Andrea, F. (2016). Northern Hemisphere atmospheric blocking representation in global climate models: Twenty years of improvements? *Journal of Climate*, *29*, 8823–8840. https://doi.org/10.1175/jcli-d-16-0242.1

Dee, D. P., Uppala, S. M., Simmons, A. J., Berrisford, P., Poli, P., Kobayashi, S., et al. (2011). The ERA-Interim reanalysis: Configuration and performance of the data assimilation system. *Quarterly Journal of the Royal Meteorological Society*, *137*, 553–597. https://doi.org/10.1002/qj.828

Drouard, M., Rivière, G., & Arbogast, P. (2013). The North Atlantic oscillation response to large-scale atmospheric anomalies in the northeastern Pacific. *Journal of the Atmospheric Sciences*, *70*, 2854–2874. https://doi.org/10.1175/jas-d-12-0351.1

Drouard, M., & Woollings, T. (2018). Contrasting mechanisms of summer blocking over western Eurasia. *Geophysical Research Letters*, *45*, 12–040. https://doi.org/10.1029/2018gl079894

Duchon, C. E. (1979). Lanczos filtering in one and two dimensions. *Journal of Applied Meteorology*, *18*, 1016–1022. https://doi.org/10.1175/1520-0450(1979)018<1016:lfioat>2.0.co;2

Franzke, C., Lee, S., & Feldstein, S. B. (2004). Is the north Atlantic oscillation a breaking wave? *Journal of the Atmospheric Sciences*, *61*, 145–160. https://doi.org/10.1175/1520-0469(2004)061<0145:itnaoa>2.0.co;2

Gollan, G., & Greatbatch, R. J. (2017). The relationship between Northern Hemisphere winter blocking and tropical modes of variability. *Journal of Climate*, *30*, 9321–9337. https://doi.org/10.1175/jcli-d-16-0742.1

Gollan, G., Greatbatch, R. J., & Jung, T. (2015). Origin of variability in northern Hemisphere winter blocking on interannual to decadal timescales. *Geophysical Research Letters*, *42*, 10–37. https://doi.org/10.1002/2015gl066572

Green, J. S. A. (1977). The weather during July 1976: Some dynamical considerations of the drought. *Weather*, *32*(4), 120–126. https://doi.org/10.1002/j.1477-8696.1977.tb04532.x

Hamill, T. M., & Kiladis, G. N. (2014). Skill of the MJO and northern Hemisphere blocking in GEFS medium-range reforecasts. *Monthly Weather Review*, *142*, 868–885. https://doi.org/10.1175/mwr-d-13-00199.1

Henderson, S. A., & Maloney, E. D. (2018). The impact of the Madden-Julian oscillation on high-latitude winter blocking during El Niño-southern oscillation events. *Journal of Climate*, *31*, 5293–5318. https://doi.org/10.1175/jcli-d-17-0721.1

Henderson, S. A., Maloney, E. D., & Barnes, E. A. (2016). The influence of the Madden-Julian oscillation on northern hemisphere winter blocking. *Journal of Climate*, *29*, 4597–4616. https://doi.org/10.1175/jcli-d-15-0502.1

Hoskins, B. J., & Sardeshmukh, P. D. (1987). A diagnostic study of the dynamics of the Northern Hemisphere winter of 1985–86. *Quarterly Journal of the Royal Meteorological Society*, *113*, 759–778. https://doi.org/10.1002/qj.49711347705

Hwang, J., Martineau, P., Son, S.-W., Miyasaka, T., & Nakamura, H. (2020). The role of transient eddies in North Pacific blocking formation and its seasonality. *Journal of the Atmospheric Sciences*, *77*, 2453–2470. https://doi.org/10.1175/jas-d-20-0011.1

Illari, L. (1984). A diagnostic study of the potential vorticity in a warm blocking anticyclone. *Journal of the Atmospheric Sciences*, *41*, 3518–3526. https://doi.org/10.1175/1520-0469(1984)041<3518:adsotp>2.0.co;2

Legras, B., & Ghil, M. (1985). Persistent anomalies, blocking and variations in atmospheric predictability. *Journal of the Atmospheric Sciences*, *42*, 433–471. https://doi.org/10.1175/1520-0469(1985)042<0433:pabavi>2.0.co;2
Mak, M. (1991). Dynamics of an atmospheric blocking as deduced from its local energetics. *Quarterly Journal of the Royal Meteorological Society*, *117*, 477–493. https://doi.org/10.1002/qj.49711749904
Martineau, P., Chen, G., & Burrows, D. A. (2017). Wave events: Climatology, trends, and relationship to Northern Hemisphere winter blocking and weather extremes. *Journal of Climate*, *30*, 5675–5697. https://doi.org/10.1175/jcli-d-16-0692.1
Masato, G., Hoskins, B. J., & Woollings, T. (2013). Winter and summer northern Hemisphere blocking in CMIP5 models. *Journal of Climate*, *26*, 7044–7059. https://doi.org/10.1175/jcli-d-12-00466.1
Masato, G., Hoskins, B. J., & Woollings, T. J. (2009). Can the frequency of blocking be described by a red noise process? *Journal of the Atmospheric Sciences*, *66*, 2143–2149. https://doi.org/10.1175/2008jas2907.1
Masato, G., Hoskins, B. J., & Woollings, T. J. (2012). Wave-breaking characteristics of midlatitude blocking. *Quarterly Journal of the Royal Meteorological Society*, *138*, 1285–1296. https://doi.org/10.1002/qj.990
Mullen, S. L. (1987). Transient eddy forcing of blocking flows. *Journal of the Atmospheric Sciences*, *44*, 3–22. https://doi.org/10.1175/1520-0469(1987)044<0003:tefobf>2.0.co;2
Murphy, J. M., Harris, G. R., Sexton, D. M. H., Kendon, E. J., Bett, P. E., Clark, R. T., et al. (2018). *UKCP18 land projections: Science report*. Retrieved from https://www.metoffice.gov.uk/pub/data/weather/uk/ukcp18/science-reports/UKCP18-Land-report.pdf
Nakamura, H., Nakamura, M., & Anderson, J. L. (1997). The role of high- and low-frequency dynamics in blocking formation. *Monthly Weather Review*, *125*, 2074–2093. https://doi.org/10.1175/1520-0493(1997)125<2074:trohal>2.0.co;2
Nakamura, N., & Huang, C. S. Y. (2018). Atmospheric blocking as a traffic jam in the jet stream. *Science*, *361*(6397), 42–47. https://doi.org/10.1126/science.aat0721
Parker, T., Woollings, T., Weisheimer, A., O'Reilly, C., Baker, L., & Shaffrey, L. (2019). Seasonal predictability of the winter North Atlantic Oscillation from a jet stream perspective. *Geophysical Research Letters*, *46*(16), 10159–10167. https://doi.org/10.1029/2019gl084402
Pelly, J. L., & Hoskins, B. J. (2003). A new perspective on blocking. *Journal of the Atmospheric Sciences*, *60*, 743–755. https://doi.org/10.1175/1520-0469(2003)060<0743:anpob>2.0.co;2
Peters, D., & Waugh, D. W. (1996). Influence of barotropic shear on the poleward advection of upper-tropospheric air. *Journal of the Atmospheric Sciences*, *53*, 3013–3031. https://doi.org/10.1175/1520-0469(1996)053<3013:iobsot>2.0.co;2
Pfahl, S., Schwierz, C., Croci-Maspoli, M., Grams, C. M., & Wernli, H. (2015). Importance of latent heat release in ascending air streams for atmospheric blocking. *Nature Geoscience*, *8*, 610–614. https://doi.org/10.1038/ngeo2487
Postel, G. A., & Hitchman, M. H. (1999). A climatology of Rossby wave breaking along the subtropical tropopause. *Journal of the Atmospheric Sciences*, *56*, 359–373. https://doi.org/10.1175/1520-0469(1999)056<0359:acorwb>2.0.co;2
Renwick, J. A., & Revell, M. J. (1999). Blocking over the South Pacific and Rossby wave propagation. *Monthly Weather Review*, *127*, 2233–2247. https://doi.org/10.1175/1520-0493(1999)127<2233:botspa>2.0.co;2
Rex, D. F. (1950). Blocking action in the middle troposphere and its effect upon regional climate. *Tellus*, *2*, 196–211. https://doi.org/10.3402/tellusa.v2i3.8546
Röthlisberger, M., & Martius, O. (2019). Quantifying the local effect of northern hemisphere atmospheric blocks on the persistence of summer hot and dry spells. *Geophysical Research Letters*, *46*, 10101–10111. https://doi.org/10.1029/2019gl083745
Sanders, F., & Gyakum, J. R. (1980). Synoptic-dynamic climatology of the 'bomb'. *Monthly Weather Review*, *108*, 1589–1606. https://doi.org/10.1175/1520-0493(1980)108<1589:sdcot>2.0.co;2
Schaller, N., Sillmann, J., Anstey, J., Fischer, E. M., Grams, C. M., & Russo, S. (2018). Influence of blocking on northern European and western Russian heatwaves in large climate model ensembles. *Environmental Research Letters*, *13*, 054015. https://doi.org/10.1088/1748-9326/aaba55
Schneidereit, A., Schubert, S., Vargin, P., Lunkeit, F., Zhu, X., Peters, D. H. W., & Fraedrich, K. (2012). Large-scale flow and the long-lasting blocking high over Russia: Summer 2010. *Monthly Weather Review*, *140*, 2967–2981. https://doi.org/10.1175/mwr-d-11-00249.1
Schwierz, C., Croci-Maspoli, M., & Davies, H. (2004). Perspicacious indicators of atmospheric blocking. *Geophysical Research Letters*, *31*. https://doi.org/10.1029/2003gl019341
Shutts, G. J. (1983). The propagation of eddies in diffluent jetstreams: Eddy vorticity forcing of blocking flow fields. *Quarterly Journal of the Royal Meteorological Society*, *109*(462), 737–761. https://doi.org/10.1002/qj.49710946204
Sousa, P. M., Trigo, R. M., Barriopedro, D., Soares, P. M. M., & Santos, J. A. (2018). European temperature responses to blocking and ridge regional patterns. *Climate Dynamics*, *50*, 457–477. https://doi.org/10.1007/s00382-017-3620-2
Steinfeld, D., & Pfahl, S. (2019). The role of latent heating in atmospheric blocking dynamics: A global climatology. *Climate Dynamics*, *53*, 6159–6180. https://doi.org/10.1007/s00382-019-04919-6
Sumner, E. J. (1954). A study of blocking in the Atlantic-European of the northern Hemisphere. *Quarterly Journal of the Royal Meteorological Society*, *80*, 402–416. https://doi.org/10.1002/qj.49708034510
Thorncroft, C. D., Hoskins, B. J., & McIntyre, M. E. (1993). Two paradigms of baroclinic-wave life-cycle behaviour. *Quarterly Journal of the Royal Meteorological Society*, *119*, 17–55. https://doi.org/10.1002/qj.49711950903
Trenberth, K. E. (1986). An assessment of the impact of transient eddies on the zonal flow during a blocking episode using localized Eliassen-Palm flux diagnostics. *Journal of the Atmospheric Sciences*, *43*, 2070–2087. https://doi.org/10.1175/1520-0469(1986)043<2070:aaotio>2.0.co;2
Tyrlis, E., & Hoskins, B. J. (2008a). Aspects of a Northern Hemisphere atmospheric blocking climatology. *Journal of the Atmospheric Sciences*, *65*(5), 1638–1652. https://doi.org/10.1175/2007jas2337.1
Tyrlis, E., & Hoskins, B. J. (2008b). The morphology of northern Hemisphere blocking. *Journal of the Atmospheric Sciences*, *65*, 1653–1665. https://doi.org/10.1175/2007jas2338.1
Uppala, S. M., KÅllberg, P. W., Simmons, A. J., Andrae, U., Bechtold, V. D. C., Fiorino, M., et al. (2005). The ERA-40 re-analysis. *Quarterly Journal of the Royal Meteorological Society*, *131*, 2961–3012. https://doi.org/10.1256/qj.04.176
Weijenborg, C., de Vries, H., & Haarsma, R. J. (2012). On the direction of Rossby wave breaking in blocking. *Climate Dynamics*, *39*, 2823–2831. https://doi.org/10.1007/s00382-012-1332-1
Woollings, T., Hoskins, B., Blackburn, M., & Berrisford, P. (2008). A new Rossby Wave-breaking interpretation of the north Atlantic oscillation. *Journal of the Atmospheric Sciences*, *65*, 609–626. https://doi.org/10.1175/2007jas2347.1
Yamazaki, K., Sexton, D. M., Rostron, J. W., McSweeney, C. F., Murphy, J. M., & Harris, G. R. (2021). A perturbed parameter ensemble of HadGEM3-GC3.05 coupled model projections: Part 2: Global performance and future changes. *Climate Dynamics*. https://doi.org/10.1007/s00382-020-05608-5